Determination of Road Profile Using Multiple Passing Vehicle Measurements

Jennifer Keenahan[a], Yifei Ren[a]* and Eugene J. OBrien[a]

[a]*School of Civil Engineering and UCD Earth Institute,*

University College Dublin, Dublin, Ireland

E-mails: jennifer.keenahan@ucd.ie, ren.yifei@ucdconnect.ie, eugene.obrien@ucd.ie

Determination of Road Profile Using Multiple Passing Vehicle Measurements

This paper describes a novel method to determine a road profile through the analysis of accelerations in a passing vehicle. A direct integration algorithm is proposed to determine the profile from the measured vehicle acceleration response. A sprung mass model and a half-car model are used to represent the vehicles in separate analyses. Combining the direct integration algorithm with the Cross Entropy (CE) optimisation method, a vehicle fleet monitoring concept is proposed for the monitoring of roads and/or bridges. In this approach, the profile can be calculated using accelerations from multiple vehicles without prior knowledge of the vehicle properties. Numerical results show that calculated profiles are the same as the 'true' profiles which were used to generate the 'simulated measured' accelerations.

Keywords: Roads & highways, Infrastructure, Damage assessment, Health & safety, Monitoring, Optimization

Introduction

Over time, roads and bridges often become damaged due to vehicle overloading, bridge strikes and due to environmental effects. Undoubtedly, this damage may impact the safe running of the transportation network and consequently, infrastructure monitoring is an important area of research. Road profiles are often monitored using profilometers, particularly for highways and major roads but these specialist vehicles are expensive and do not run frequently. Highway structures such as bridges are most commonly monitored by visual inspection that requires large numbers of inspectors and significant cost. Furthermore, due to human subjectivity and differing experience, it is often difficult to achieve consistency in the results.

Recently, the concept of sensor-based monitoring of road structures has become popular in the literature. It can be divided into two types: direct and indirect monitoring. Direct monitoring measures the response directly using sensors installed in the structure. This method requires multiple sensors to be mounted on a bridge, got example, which can be more expensive

than traditional visual inspections. It also results in a significant amount of data being collected, stored, transmitted and processed. Furthermore, the direct sensing method is specific to the infrastructure in which the sensors are installed; these sensors cannot be subsequently reused in another structure. As a result, the concept of indirect monitoring (the 'drive-by' method) is proposed by Yang, Lin, & Yau (2004), Yang and Lin (2005) and González, OBrien, Li, & Cashell (2008). This family of methods uses inertial sensors installed in a passing vehicle to assess the condition of pavement, railway track or a bridge indirectly. There is no need for sensors to be installed in the road or on the bridge. This paper proposes a new method of drive-by monitoring to determine the surface profile. For a road pavement or railway track, this can be used directly as a measure of pavement/track condition. For a bridge, the profile experienced by the vehicle includes elements of bridge deflection and, as such, can be used as an indication of the bridge condition. Compared to the direct method, indirect monitoring has a number of advantages; it is easy to operate, efficient, economic, and no power supply is needed in the infrastructure.

The drive-by technique is often used in bridge monitoring. Malekjafarian, McGetrick, & OBrien (2015) present a review of the state-of-the-art for highway bridges. Most indirect methods infer dynamic characteristics of the bridge from responses measured on the vehicle, such as natural frequency, damping or mode shapes (McGetrick, González, & Obrien, 2009; Yang, Li, & Chang, 2014; Yang, et al., 2004). Many researchers extend these concepts in laboratory experiments and field tests to verify the drive-by inspection approach for bridges (Kim et al., 2011; Lin and Yang, 2005). Some methods seek to detect bridge damage directly according to the profile. OBrien and Keenahan (2015) introduce the concept of 'apparent profile'. The results show that the time-shifted difference in the apparent profile can be used as a damage indicator for the bridge. Elhattab, Uddin, & OBrien (2016) use truck acceleration

histories to calculate the Bridge Displacement Difference Profile (BDDP) which is shown to be sensitive to structural damage.

In recent years, different methods have been proposed to measure road surface profiles using drive-by techniques. The concept of using crowd sourcing to detect potholes or bumps in pavements is already established in the 'Street Bump' app in operation in Boston. However, this is a very simple empirical approach, most likely using an acceleration threshold in the smartphone, above which a bump is registered. There are also some challenges with this concept. For example, the quality of devices can limit the quality of the gathered information, compromising the precision (O'Leary, 2013). Souza, Giusti, & Batista (2018) introduce a new system, Asfault, to evaluate and monitor road pavement condition using smartphone sensors. These sensors can measure the vehicle vibration while driving and use the data to evaluate pavement condition. This system classifies road quality into 4-classes: Good, Average, Fair, and Poor, as well as identifying the occurrence of obstacles on the road. Zang, Shen, Huang, Wan, & Shi (2018) use GPS and accelerometer sensors on bicycle-mounted smartphones to measure the road surface roughness of pedestrian and bicycle lanes. However, smartphone-based sensing has the challenges of low frequency and low detection accuracy (Sattar, Li, & Chapman, 2018). Sayers and Karamihas (1996), (1998) discuss inertial profilometers, that can measure profiles at highway speeds. A typical inertial profilometer consists of a vehicle equipped with a height sensing device, such as a laser, which measures pavement elevations at regular intervals. The effects of the vehicle can be removed from the elevation measurements using accelerometer(s) mounted on the vehicle. High resolution profile measurements can be provided, but at significant cost because of the laser-based technology. Ergun, Iyinam, & Iyinam (2005) also measure road surface macrotexture with a laser profilometer. Ma et al. (2018) review developments in mobile laser scanning (MLS) techniques which introduce many

MLS technology applications and show that this technology is can achieve accurate road condition detection.

With considerably greater precision (and cost), Flintsch et al. (2012) identify continuous deflection devices such as traffic speed deflectometers (TSD's), as valuable tools in pavement analysis. Using a set of velocity-sensing lasers, the TSD measures the pavement deflection velocity based on the Doppler principle. Malekjafarian, Martinez, & OBrien (2017) use a vehicle pavement interaction model to illustrate the functionality of a TSD. The pavement is represented by a Winkler model and pavement deflections are calculated from the simulated TSD measurements. The deflections compare well to those from a numerical model. Later, OBrien and Keenahan (2015) propose a TSD-type vehicle containing two displacement sensors to measure pavement deflection. Using data collected from sensors in the TSD, the 'apparent profile' is calculated and the time-shifted difference in the apparent profile is used to indicate bridge damage. Numerical simulation suggests that this method can be used as a damage indicator in the presence of noise. It is shown to be economical, efficient and free from the influence of other heavy traffic on the bridge.

Accelerometer(s) mounted on the vehicle provide an accurate means to monitor road profile at low cost. Imine, Delanne, & M'Sirdi (2006) present a method to estimate road profile by analysing the measured dynamic response of an instrumented vehicle. In this method, a full car sprung mass model is used to determine the road profile from the vertical wheel accelerations and vertical displacement and rotation of the vehicle body. González, et al. (2008) collect data from accelerometers fitted to a vehicle and use this data to estimate the condition of a road. This approach uses the relationship between vehicle accelerations and the power spectral densities of road surfaces using a transfer function. The road condition is classified using Fourier analysis to calculate the power spectral density (PSD) function of the surface. The result shows that road profile roughness can be accurately classified using axle and body

accelerations from a range of simulated vehicle–road dynamic scenarios. Harris, Gonzalez, OBrien, & McGetrick (2010) describe a novel method for the characterisation of road surface profiles using measurements of vehicle acceleration. The method proposes the use of a combinatorial optimisation technique to determine the road profile which causes a set of observed responses in a known vehicle model. The parameters of the half-car model are determined using road profiles and known accelerations. The algorithm is numerically validated for different road profiles and, while computationally intensive, the calculated road profile heights are found to provide a good fit to the true profiles. OBrien, McGetrick, & Gonzalez (2014) present a method to monitor transport infrastructure (such as bridges and pavements) by analysing vehicle accelerations. Using the vehicle response, an algorithm is developed to identify the dynamic vehicle-bridge interaction forces. It is proposed that this method could be used to identify the global bending stiffness of the bridge and to predict the pavement roughness. Fauriat, Mattrand, Gayton, Beakou, & Cembrzynski (2016) use a data processing algorithm to estimate road profiles from the dynamic responses measured on a vehicle. This algorithm, based on Kalman filtering theory, aims at solving a so-called inverse problem, in a stochastic framework. The application of Kalman filters was investigated to classify road condition by Wang et al. (2016). Fox, Kumar, Chen, & Bai (2017) develop a novel crowd-sourced system to monitor the road. This method uses accelerometer data from embedded vehicle sensors to detect and localize potholes in multi-lane environments. An Independent Component Analysis (ICA) technique is used to identify the road profile knowing the dynamic responses of the system (Ben Hassen et al., 2019).

Cross Entropy (CE) optimisation is sometimes used to solve optimisation problems in Civil Engineering. Walsh and González (2009) use CE optimisation to estimate the stiffness distribution of a structure, given a set of displacements. Harris, et al. (2010) use CE optimisation to infer the parameters of a vehicle model by examining the vertical acceleration

response of the vehicle to a known excitation. Li, Jiang, Wang, & Zhu (2014) develop an optimization method to identify 1st frequency and stiffness of the bridge based on a Generalized Pattern Search Algorithm (GPSA). OBrien and Keenahan (2015) use CE optimisation to determine the apparent profile, where displacements recorded by the sensors are the assumed inputs. Quirke, Cantero, OBrien, & Bowe (2016) use the CE optimisation technique to determine the track stiffness profile of a railway track. This method generates a vehicle response that best fits the measured vertical accelerations of a railway carriage bogie.

While the use of CE optimisation methods represents a step forward in solving engineering problems, the computational effort of doing so is a significant drawback. It is often grossly inefficient to solve engineering problems using optimisation in a brute-force manner. This paper introduces a new indirect method of back-calculating the road profile from vehicle accelerations. Firstly, the paper presents the direct integration algorithm for calculating the road profile using the vehicle acceleration histories. The work is then expanded to introduce the concept of using a fleet of vehicles to find the road profile more accurately, ever without prior knowledge of the vehicle properties. This fleet-based monitoring method uses the direct integration and the CE algorithms together.

MODEL DESCRIPTION

Vehicle model

In this study, a variety of vehicle models are used. Initially, the work considers a sprung mass model, then a half-car model to represent vehicles travelling on profiles.

Sprung mass model

Firstly, the vehicle is represented as a sprung mass model, as shown in Figure 1. This simple dynamic system consists of a mass and a spring. The general equation of this single degree of

freedom dynamical system can be expressed as:

$$m\ddot{u} + ku = F \tag{1}$$

where m and k are the mass and stiffness of the vehicle, respectively, $\ddot{u}$ and u are the vehicle acceleration and displacement respectively, and F is the applied force at the vehicle degree of freedom, ie, the force in the spring. F is related to profile $y(t)$ and can be expressed as:

$$F(t) = k \times y(t) \tag{2}$$

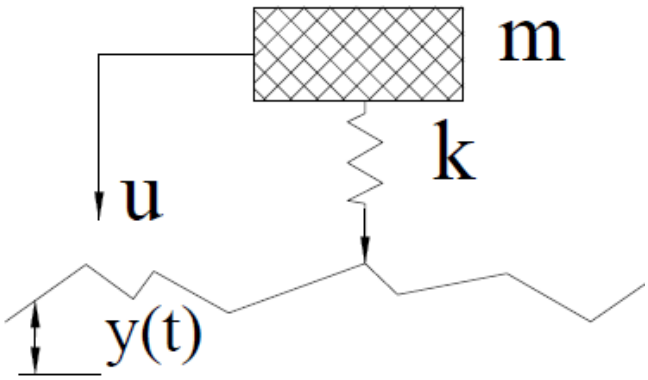

Figure 1. Sprung mass and profile model.

Half-car model

The vehicle is later extended to a 4 degree-of-freedom half-car model travelling on the road (Figure 2). The four independent degrees of freedom correspond to sprung mass bounce displacement, u_s sprung mass pitch rotation, θ_s and axle hop displacements of the unsprung masses at axle 1 and axle 2, u_{u1} and u_{u2} respectively. The sprung mass, m_s represents the vehicle body and I_s is the sprung mass moment of inertia. The unsprung masses, $m_{u,1}$ and $m_{u,2}$ represent the axle components. The sprung mass connects to the axle masses via a combination of springs and dampers. The stiffness of springs is $K_{s,i}$ and damping coefficients of viscous dampers are $C_{s,i}$ which represent the suspension components for the front and rear axles ($i =$

1,2). The axle masses connect to the road surface via springs with linear stiffnesses, $K_{t,i}$ which represent the tyre components for the front and rear axles ($i = 1,2$). Finally, the distances from the axles to the centre of gravity are D_1 and D_2.

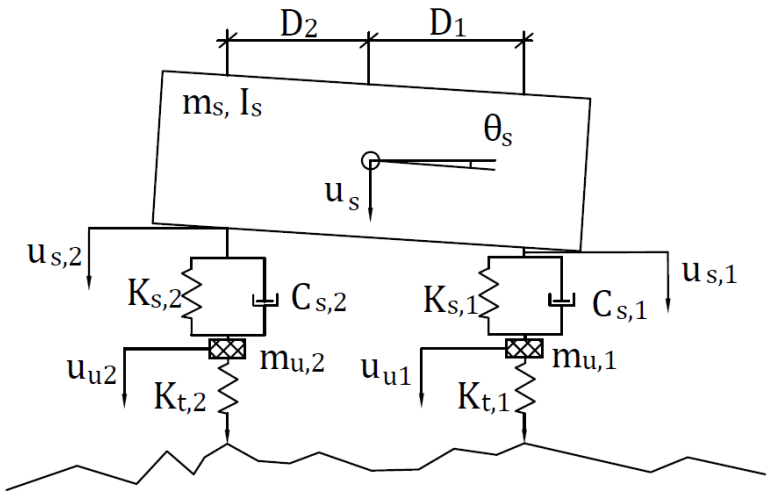

Figure 2. Half-Car and road model.

The equations of motion of the vehicle are obtained by imposing equilibrium of all forces and moments acting it:

$$M_v\ddot{u}_v + C_v\dot{u}_v + K_v u_v = f_v \tag{3}$$

where M_v, C_v, and K_v are the mass, damping and stiffness matrices of the vehicle respectively:

$$\mathrm{M_v} = \begin{bmatrix} m_s & 0 & 0 & 0 \\ 0 & I_s & 0 & 0 \\ 0 & 0 & m_{u,1} & 0 \\ 0 & 0 & 0 & m_{u,2} \end{bmatrix} \tag{4}$$

$$C_v = \begin{bmatrix} C_{s,1} + C_{s,2} & D_1C_{s,1} - D_2C_{s,2} & -C_{s,1} & -C_{s,2} \\ D_1C_{s,1} - D_2C_{s,2} & {D_1}^2C_{s,1} + {D_2}^2C_{s,2} & -D_1C_{s,1} & D_2C_{s,2} \\ -C_{s,1} & -D_1C_{s,1} & C_{s,1} & 0 \\ -C_{s,2} & D_2C_{s,2} & 0 & C_{s,2} \end{bmatrix} \tag{5}$$

$$K_{\boldsymbol{v}} = \begin{bmatrix} K_{s,1} + K_{s,2} & D_1K_{s,1} - D_2K_{s,2} & -K_{s,1} & -K_{s,2} \\ D_1K_{s,1} - D_2K_{s,2} & {D_1}^2K_{s,1} + {D_2}^2K_{s,2} & -D_1K_{s,1} & D_2K_{s,2} \\ -K_{s,1} & -D_1K_{s,1} & K_{s,1}+K_{t,1} & 0 \\ -K_{s,2} & D_2K_{s,2} & 0 & K_{s,2}+K_{t,2} \end{bmatrix} \quad (6)$$

The vectors, $\ddot{u}_v$, $\dot{u}_v$ and u_v are vehicle accelerations, velocities and displacements respectively. The displacement vector of the vehicle is:

$$u_v = \{u_s, \theta_s, u_{u1}, u_{u2}\}^T \quad (7)$$

The time-varying dynamic interaction force vector is:

$$f_v = \{0,0, F_{t1}, F_{t2}\}^T \quad (8)$$

The dynamic interaction force at wheel i is:

$$F_{ti} = K_{t,i} \times y_i \quad (9)$$

$i = 1,2$, where y_i is the road profile.

Road model

In this research, a 100 m road profile is generated by Monte Carlo simulation according to the ISO standard (ISO 8608: 1995) . A class 'A' road is used which is a 'very good' profile and expected in a well-maintained highway. It has a geometric spatial mean of $16 \times 10^{-6} m^3/$ cycle. A moving average filter is applied to the generated road profile heights, y_i. It is over a distance of 0.24 m to simulate the attenuation of short wavelength disturbances by the tyre contact patch (Harris, OBrien, & González, 2007; OBrien, et al., 2014).

Direct solution of profile calculation

In vehicle-road-interaction, the forward problem uses the coupled vehicle-road model to find vehicle accelerations, velocities and displacements for a specified road profile. By contrast, the inverse problem takes measured accelerations from a vehicle traversing a road, $\ddot{u}$ and uses this

signal to find the road profile.

In previous research, the road profiles are back-calculated from vehicle-mounted sensor data (accelerations) using an optimisation procedure (e.g., OBrien and Keenahan, 2015). This method involves finding the profile elevations that give a best fit to the measured acceleration data. In this section, a new direct integration approach is developed and used to solve the inverse problem of finding the road profile from vehicle acceleration histories. The dynamic systems are solved in MATLAB using the Newmark-Beta integration scheme for sprung mass and half-car models.

Sprung mass model

For the sprung mass vehicle, the inverse problem is solved using the Newmark-Beta method. A value of $\gamma = 0.8$ is used to ensure unconditional stability of the algorithm. In the Newmark-Beta method, the integration constants are listed:

$$\text{Time step, } \Delta t = 0.001,\ \ \gamma = 0.8, \beta = \ 0.25 \times (0.5 + \gamma)^2$$

$$a_0 = 1/(\beta \times \Delta t^2)\,, \qquad a_1 = \gamma/(\beta \times \Delta t)\,, \qquad a_2 = 1/(\beta \times \Delta t),$$

$$a_3 = 1/(\beta \times 2) - 1, a_4 = \gamma/\beta - 1, \tag{10}$$

$$a_5 = \Delta t/2 \times (\gamma/\beta - 2), a_6 = (1 - \gamma) \times \Delta t, a_7 = \ \gamma \times \Delta t$$

At the first time step, the mass, m, spring stiffness, k, time step, Δt, initial displacement and velocity of the mass, $u_0, \dot{u}_0,$ are deemed to be known. The acceleration of the mass $\ddot{u}$ is measured so it is also known for each time step. Here the displacement and velocity of the mass at each time step can be calculated using the Newmark-Beta method:

$$u_{t+\Delta t} = (\ddot{u}_{t+\Delta t} + a_2 \times \dot{u}_t + a_3 \times \ddot{u}_t)/a_0 + u_t \tag{11}$$

$$\dot{u}_{t+\Delta t} = \dot{u}_t + a_6 \times \ddot{u}_t + a_7 \times \ddot{u}_{t+\Delta t} \tag{12}$$

Using the displacement, velocity and acceleration of the mass, the force being applied to the mass can be determined.

The effective stiffness matrix is found using:

$$\bar{K} = k + a_0 \times m \tag{13}$$

The effective force is found using:

$$\bar{F}_{t+\Delta t} = \bar{K} \times u_{t+\Delta t} \tag{14}$$

$$F_{t+\Delta t} = \bar{F}_{t+\Delta t} - m \times (a_0 \times u_t + a_2 \times \dot{u}_t + a_3 \times \ddot{u}_t) \tag{15}$$

Finally, the profile is calculated using:

$$y_{t+\Delta t} = F_{t+\Delta t}/k \tag{16}$$

Figure 3 shows a sample 'calculated' profile using this direct-integration inverse method, and the 'true' profile which was used to generate the accelerations in the forward problem. In both cases, the mass of the vehicle is 15 000 kg and stiffness of the spring is 3 500×10^3 Nm^{-1}. The results clearly demonstrate that the calculated profile is the same as the 'true' profile.

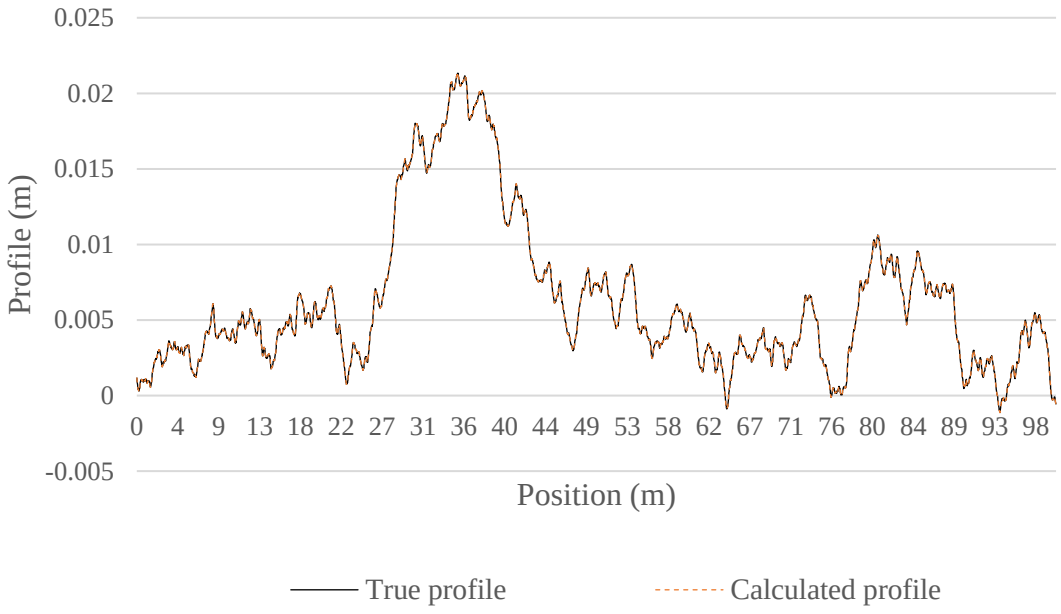

Figure 3. Calculated profile and true profile of sprung mass model.

Half-Car model

In later simulations, the vehicle is represented with a half-car model, and the inverse problem is also solved using the Newmark-Beta method. The approach assumes knowledge of the sprung mass bounce acceleration, $\ddot{u}$, and the sprung mass pitch rotational velocity $\dot{\theta}_s$. Also, the vehicle properties $\mathrm{M}_v, C_v, \mathrm{K}_v$ are taken to be known. Then, using the Newmark-Beta integration scheme, the displacement and velocity of the sprung mass can be calculated. The unsprung mass displacement can be calculated using the equations of motion of the sprung mass. Then, the acceleration and velocity of the unsprung mass can be found. Finally, using the Newmark-Beta integration scheme, the time varying interaction forces applied by the vehicle and the profile can be calculated. There are five steps in the process as follows:

Step1:

Using the Newmark-Beta integration scheme, the sprung mass bounce displacement, u_s, and velocity, $\dot{u}_s$, sprung mass pitch rotational displacement, θ_s, and accelerations, $\ddot{\theta}_s$, can be calculated:

$$u_{s,t+\Delta t} = (\ddot{u}_{s,t+\Delta t} + a_2 \times \dot{u}_{s,t} + a_3 \times \ddot{u}_{s,t})/a_0 + u_{s,t} \tag{17}$$

$$\dot{u}_{s,t+\Delta t} = \dot{u}_{s,t} + a_6 \times \ddot{u}_{s,t} + a_7 \times \ddot{u}_{s,t+\Delta t} \tag{18}$$

$$\theta_{s,t+\Delta t} = (\dot{\theta}_{s,t+\Delta t} + a_4 \times \dot{\theta}_{s,t} + a_5 \times \ddot{\theta}_{s,t})/a_1 + \theta_{s,t} \tag{19}$$

$$\ddot{\theta}_{s,t+\Delta t} = a_0 \times (\theta_{s,t+\Delta t} - \theta_{s,t}) - a_2 \times \dot{\theta}_{s,t} - a_3 \times \ddot{\theta}_{s,t} \tag{20}$$

Step2:

According to Equations (3) to (9), the equations of motion of the sprung mass can be found:

$$m_s \times \ddot{u}_{s,t+\Delta t} + \left(C_{s,1} + C_{s,2}\right) \times \dot{u}_{s,t+\Delta t} + (D_1 C_{s,1} - D_2 C_{s,2}) \times \dot{\theta}_{s,t+\Delta t} - C_{s,1} \times \dot{u}_{u1,t+\Delta t}$$

$$-C_{s,2} \times \dot{u}_{u2,t+\Delta t} + \left(K_{s,1} + K_{s,2}\right) \times u_{s,t+\Delta t} + (D_1 K_{s,1} - D_2 K_{s,2}) \times \theta_{s,t+\Delta t}$$

$$-K_{s,1} \times u_{u1,t+\Delta t} - K_{s,2} \times u_{u2,t+\Delta t} = 0 \quad (21)$$

$$I_s \times \ddot{\theta}_{s,t+\Delta t} + \left(D_1 C_{s,1} - D_2 C_{s,2}\right) \times \dot{u}_{s,t+\Delta t} + ({D_1}^2 C_{s,1} + {D_2}^2 C_{s,2}) \times \dot{\theta}_{s,t+\Delta t}$$

$$-D_1 C_{s,1} \times \dot{u}_{u1,t+\Delta t} + D_2 C_{s,2} \times \dot{u}_{u2,t+\Delta t} + \left(D_1 K_{s,1} - D_2 K_{s,2}\right) \times u_{s,t+\Delta t}$$

$$+({D_1}^2 K_{s,1} + {D_2}^2 K_{s,2}) \times \theta_{s,t+\Delta t} - D_1 K_{s,1} \times u_{u1,t+\Delta t} + D_2 K_{s,2} \times u_{u2,t+\Delta t} = 0 \quad (22)$$

The terms, $\dot{u}_{u2,t+\Delta t}$ and $u_{u2,t+\Delta t}$ can be removed by combining Equations (22) with Equations (21), scaled by D_2:

$$D_2 m_s \times \ddot{u}_{s,t+\Delta t} + D_2\left(C_{s,1} + C_{s,2}\right) \times \dot{u}_{s,t+\Delta t} + D_2(D_1 C_{s,1} - D_2 C_{s,2}) \times \dot{\theta}_{s,t+\Delta t} + D_2\left(K_{s,1} + K_{s,2}\right) \times u_{s,t+\Delta t} + D_2(D_1 K_{s,1} - D_2 K_{s,2}) \times \theta_{s,t+\Delta t} + I_s \times \ddot{u}_{s,t+\Delta t} + \left(D_1 C_{s,1} - D_2 C_{s,2}\right) \times \dot{u}_{s,t+\Delta t} + ({D_1}^2 C_{s,1} + {D_2}^2 C_{s,2}) \times \dot{\theta}_{s,t+\Delta t} + \left(D_1 K_{s,1} - D_2 K_{s,2}\right) \times u_{s,t+\Delta t} + ({D_1}^2 K_{s,1} + {D_2}^2 K_{s,2}) \times \theta_{s,t+\Delta t} = \left(D_2 C_{s,1} + D_1 C_{s,1}\right) \times \dot{u}_{u1,t+\Delta t} + (D_2 K_{s,1} + D_1 K_{s,1}) \times u_{u1,t+\Delta t} \quad (23)$$

In the Newmark-Beta method,

$$\dot{u}_{u1,t+\Delta t} = a_1 \times (u_{u1,t+\Delta t} - u_{u1,t}) - a_4 \times \dot{u}_{u1,t} - a_5 \times \ddot{u}_{u1,t} \quad (24)$$

Substituting (24) into (23), the unsprung mass displacement can be found:

$$u_{u1,t+\Delta t} = \left(D_2 m_s \times \ddot{u}_{s,t+\Delta t} + I_s \times \ddot{\theta}_{s,t+\Delta t} + \left(D_2 C_{s,1} + D_1 C_{s,1}\right) \times \dot{u}_{s,t+\Delta t} + (D_2 D_1 C_{s,1} + {D_1}^2 C_{s,1}) \times \dot{\theta}_{s,t+\Delta t} + \left(D_2 K_{s,1} + D_1 K_{s,1}\right) \times u_{s,t+\Delta t} + (D_2 D_1 K_{s,1} + {D_1}^2 K_{s,1}) \times \theta_{s,t+\Delta t} + \left(D_2 C_{s,1} + D_1 C_{s,1}\right) \times \left(a_1 \times u_{u1,t} + a_4 \times \dot{u}_{u1,t} + a_5 \times \ddot{u}_{u1,t}\right)\right) / (D_2 K_{s,1} + D_1 K_{s,1} + (D_2 C_{s,1} + D_1 C_{s,1}) \times a_1) \quad (25)$$

Step3:

Using the Newmark-Beta method, unsprung mass acceleration and velocity can be calculated:

$$\ddot{u}_{u1,t+\Delta t} = a_0 \times (u_{u1,t+\Delta t} - u_{u1,t}) - a_2 \times \dot{u}_{u1,t} - a_3 \times \ddot{u}_{u1,t} \quad (26)$$

$$\dot{u}_{u1,t+\Delta t} = \dot{u}_{u1,t} + a_6 \times \ddot{u}_{u1,t} + a_7 \times \ddot{u}_{u1,t+\Delta t} \quad (27)$$

Step4:

Use Newmark-Beta to calculate $f_{v,t+\Delta t}$ at time step, $t + \Delta t$,

The effective stiffness matrix is:

$$\overline{K} = K_v + a_0 \times M_v + a_1 \times C_v \quad (28)$$

The effective force is:

$$\bar{f}_{v,t+\Delta t} = \overline{K} \times u_{v,t+\Delta t} \quad (29)$$

and,

$$f_{v,t+\Delta t} = \bar{f}_{v,t+\Delta t} - \mathrm{M}_v \times \left(a_0 \times u_{v,t} + a_2 \times \dot{u}_{v,t} + a_3 \times \ddot{u}_{v,t}\right) - C_v \times (a_1 \times u_{v,t} + a_4 \times \dot{u}_{v,t} + a_5 \times \ddot{u}_{v,t}) \quad (30)$$

According to Equation (8), $f_{v,t+\Delta t} = \{0,0, F_{t1,t+\Delta t}, F_{t2,t+\Delta t}\}^T$, and $F_{ti,t+\Delta t}$ is known.

Step5:

Finally, the profile can be calculated using Equation (9):

$$y_{i,t+\Delta t} = F_{ti,t+\Delta t}/K_{t,i} \quad (31)$$

Using this direct integration approach, the profile can be calculated step by step. For a specified

profile, the forward problem is used here to calculate the accelerations and rotational velocities in the usual way. All the vehicle property values are listed in Table 1. These accelerations and rotational velocities are then used as the 'measurements' in a test of the inverse problem. The inverse problem is solved to back-calculate the profile using these signals. Figure 4(a) presents the calculated profile and the true profile. Figure 4(b) shows a detail in the 45 m to 55 m zone. As expected, the results show that the profile is found with a high degree of accuracy. The profiles are calculated using this approach directly. However, in the optimisation method the profiles are split into a number of phases to be calculated separately (OBrien and Keenahan, 2015). In each phase, a large population of unknows is generated and regenerated for many generations. This direct integration approach is much more efficient than an optimisation algorithm and allows the calculation to be completed in a fraction of the time.

Table 1. Vehicle parameters of half-car model.

Property	Unit	Symbol	Value
Body mass	kg	m_s	16200
Axle mass	kg	m_{u1}	700
		m_{u2}	1100
Suspension stiffness	$\mathrm{Nm^{-1}}$	$K_{s,1}$	4×10^5
		$K_{s,2}$	1×10^6
Suspension damping	$\mathrm{N\ sm^{-1}}$	$C_{s,1}$	1×10^4
		$C_{s,2}$	2×10^4
Tyre stiffness	$\mathrm{Nm^{-1}}$	$K_{t,1}$	1.75×10^6
		$K_{t,2}$	3.5×10^6
Pitch moment of inertia	$\mathrm{kg\ m^2}$	I_s	93457
Distance of axle to centre of gravity	m	D_1	2.375
		D_2	2.375

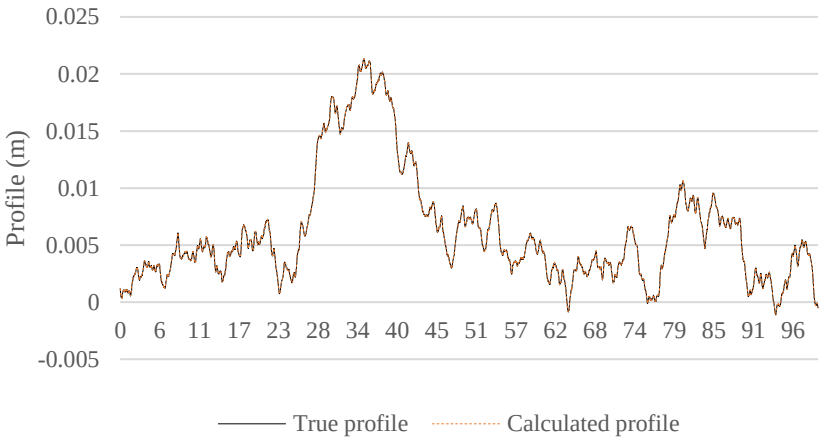

(a)

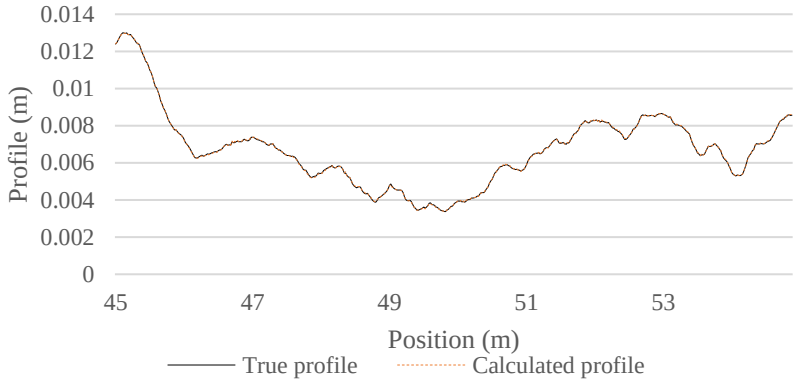

(b)

Figure 4(a). Calculated profile and true profile of half-car model (0 to 100 m).

(b). Calculated profile and true profile of half-car model (45 to 55 m).

Vehicle fleet monitoring concept

It is shown in the previous section that road profiles can be found, knowing the vehicle accelerations and the vehicle properties. In this section, a vehicle fleet monitoring concept is introduced to calculate profiles from vehicle accelerations without prior knowledge of the vehicle properties. For a single vehicle, either the profile or the vehicle properties can be found, but not both. But all vehicles in a fleet are subject to the same profile. This feature is exploited here to find the profile. To solve the fleet problem, the direct integration approach and the Cross Entropy (CE) optimisation technique are used together. Like the genetic algorithms (Goldberg

and Holland, 1988), CE is a population-based method of optimisation (Rubinstein and Kroese, 2004). A population of trial solutions is generated randomly using Monte Carlo simulation. Each solution in the population is assessed and an 'elite set' of the best solution identified. Discarding all other solutions, the vector mean and standard deviation of the 'elite set' is used to generate a new population of solution and the process repeated until convergence. It can occur that the CE algorithm converges prematurely and not converge to the true optimum. A method called 'injection' is used to address this problem, proposed by Botev and Kroese (2004). Injection resets the standard deviation in the Monte Carlo simulation to restart the algorithm. The first two injections reset the standard deviations at their initial values. Then the magnitude of the following ones decrease in inverse proportion to the number of injections (Casero, González, & Covián, 2014).

The responses to a group of vehicles whose properties are unknown provide the data used in this method. Applying CE, a population of vehicle properties are randomly generated from a normal distribution. For each vehicle in this population, the responses are used to calculate the profile using the direct integration approach. These calculated profiles will not, generally, be correct as incorrect vehicle properties have been used. However, the sets of properties for some vehicles will be better than for others and these can be identified as the corresponding profiles will be similar. The objective function for the j^{th} trial solution, O_j, is therefore the sum of squared differences of the profile its mean values.

$$O_j = \sum_i \sum_k \left(r_{i,j,k} - \bar{r}_{j,k}\right)^2 \tag{32}$$

where $r_{i,j,k}$ is the k^{th} profile elevation in the j^{th} trial of the i^{th} vehicle in the fleet,

and $\bar{r}_{j,k}$ is mean profile in the j^{th} trial of the n_i vehicles of the fleet:

$$\bar{r}_{j,k} = \frac{1}{n_i} \sum_{i} r_{i,j,k} \tag{33}$$

The objective functions are then ranked and the 10% best of the trial vehicle property sets are selected. Through the normal CE method, Monte Carlo simulation is used to generate the next generation of trial vehicle properties from the means and standard deviations of this elite set, μ and σ. Figure 5 illustrates the workflow of the algorithm presented in this paper.

Results for sprung mass modal

For this investigation a very small population of just 6 vehicles is selected to illustrate the procedure ($n_i = 6$). The parameters for these 6 vehicles are chosen randomly and used in the forward problem to generate the responses that would be measured. The six sets of parameters are given in Table 2. Using these parameters, the forward problems are solved to determine the acceleration histories. These accelerations are used as inputs to solve vehicle fleet problem. The profile is calculated using these accelerations without knowledge of the vehicle properties.

Table 2. Vehicle parameters.

	Vehicle 1	Vehicle 2	Vehicle 3	Vehicle 4	Vehicle 5	Vehicle 6
m (kg)	15 614	12 365	18 115	13 081	13 609	13 975
k (N m^{-1})	2 655×10^3	4 138×10^3	2 123×10^3	4 402×10^3	1 108×10^3	1 917×10^3

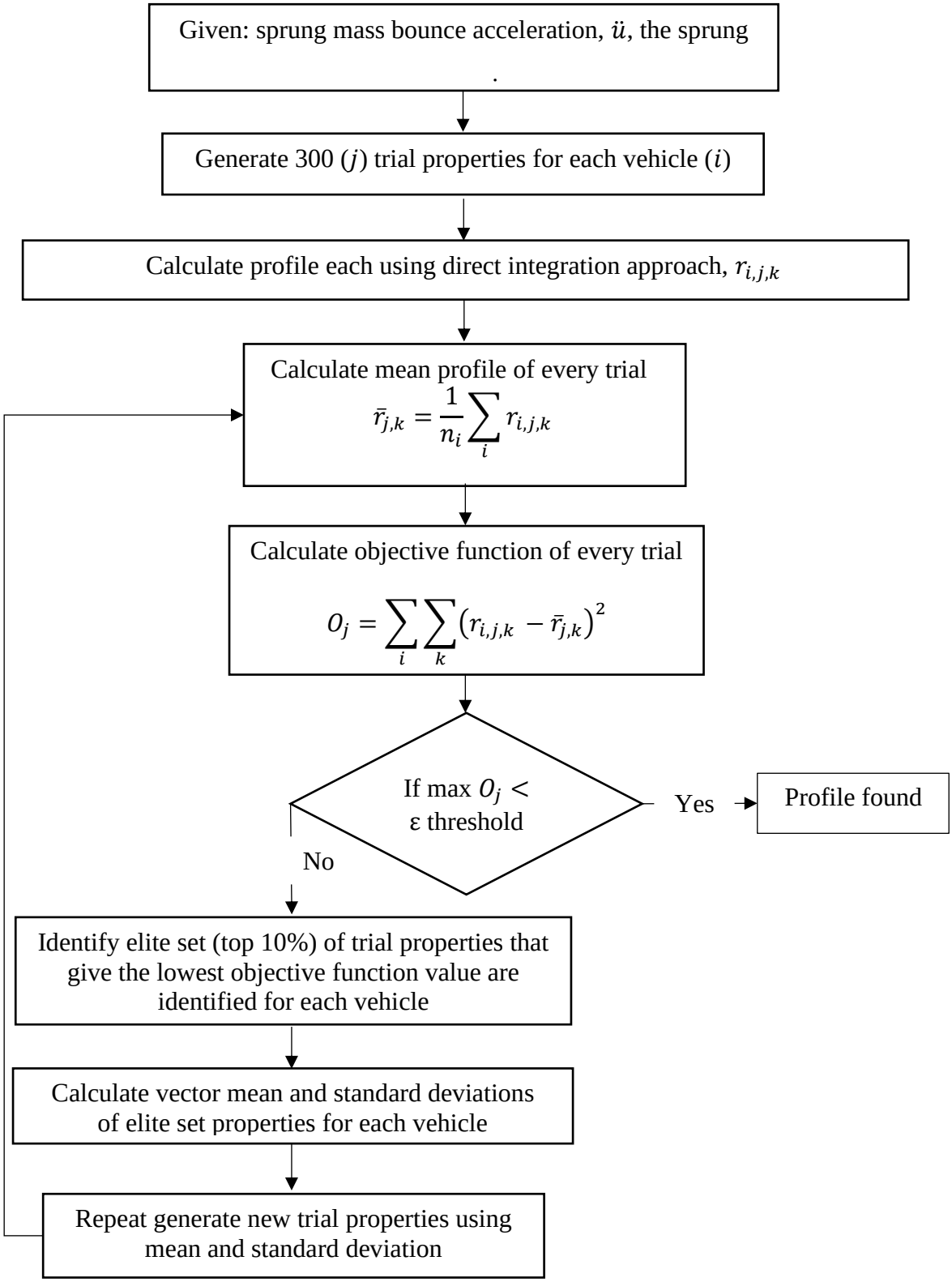

Figure 5. CE optimisation method algorithm.

The initial mean of mass and stiffness are 10000 kg and 300×10^3 Nm^{-1} respectively. The calculated profiles are shown in Figure 6 and can be seen to be the same as the true profile. The calculated parameters (m and k) for the six vehicles are highly inaccurate, as shown in Table 3 (However m/k ratio is found with good accuracy).

Table 3. Calculated vehicle parameters.

	True m (kg)	True k (Nm^{-1})	True ratio m/k	Calculated m (kg)	Calculated k (Nm^{-1})	Calculated ratio m/k
Vehicle 1	15 614	$2\,655\times10^3$	0.0059	2 098	356 920	0.0059
Vehicle 2	12 365	$4\,138\times10^3$	0.0030	1 933	645 469	0.0030
Vehicle 3	18 115	$2\,123\times10^3$	0.0085	4 221	495 372	0.0085
Vehicle 4	13 081	$4\,402\times10^3$	0.0030	1 663	558 487	0.0030
Vehicle 5	13 609	$1\,108\times10^3$	0.0123	5 524	449 414	0.0123
Vehicle 6	13 975	$1\,917\times10^3$	0.0073	3 832	523 167	0.0073

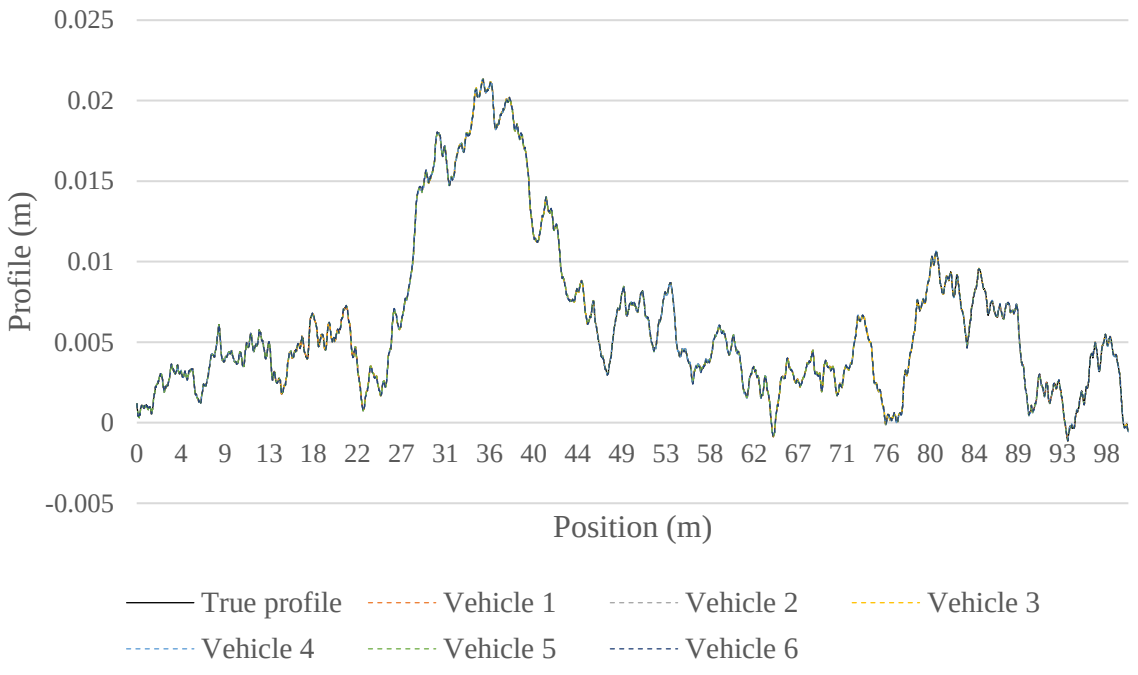

Figure 6. True profile and calculated profiles for vehicles of the fleet.

To investigate the accuracy issue, different vehicle fleets are generated. For every (m_0, k_0) pair, a local vehicle fleet of just four vehicles is generated in the immediate vicinity.

The four vehicles are $(m_0 + \Delta m, k_0), (m_0, k_0 - \Delta k), (m_0 - \Delta m, k_0),\ (m_0, k_0 + \Delta k)$, where Δm =1000 kg and Δk=100 000 Nm^{-1}. The pairs are generated by varying the mass, m_0, from 11 000 kg through 20 000 kg in increments of 1000 kg and the stiffness k_0 is generated in the immediate vicinity from 3.2×10^6 Nm^{-1} through 5×10^6 Nm^{-1} in increments of 200 000 Nm^{-1}. Using these known vehicle fleets, the objective function of Equation (32) is calculated. The accelerations used are calculated by the forward problem and the true (m_0, k_0) pair for all cases is $(14\ 000, 3.5 \times 10^6)$ whose m_0/k_0 ratio is 0.0040.

Contours of the objection function contouring are shown in Figure 7. It can be seen that there are equally good solutions for all (m_0, k_0) pairs for which the m_0/k_0 ratio is 0.0040, showing that there is insufficient information to find unique value for m_0 and k_0. Two points are chosen to solve the inverse problem to find the profiles. Point A is $(18\ 000, 4.5 \times 10^6)$ and has the same m_0/k_0 ratio as the true vehicle. Point B $(13\ 000, 3.8 \times 10^6)$, on the other hand, has a different m_0/k_0 ratio.

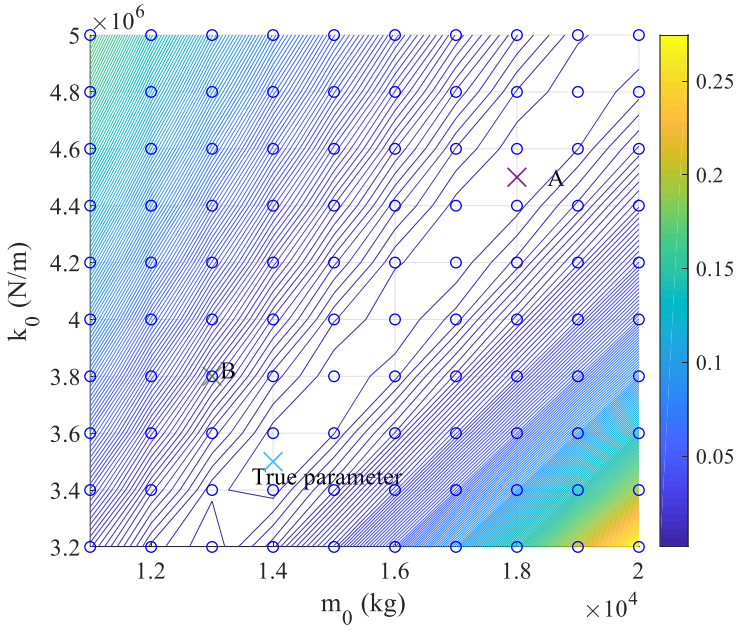

Figure 7. Objective function contours.

The calculated profiles and true profiles (0 to 100 m) are shown in Figures 8(a) and 9(a). Figures 8(b) and 9(b) show the detail in the 45 m to 55 m zone. The profile calculated at Point A is the same as the true profile even though the m and k values are different. The profile calculated at Point B is different from true profile and significantly, the 4 profiles are different from each other.

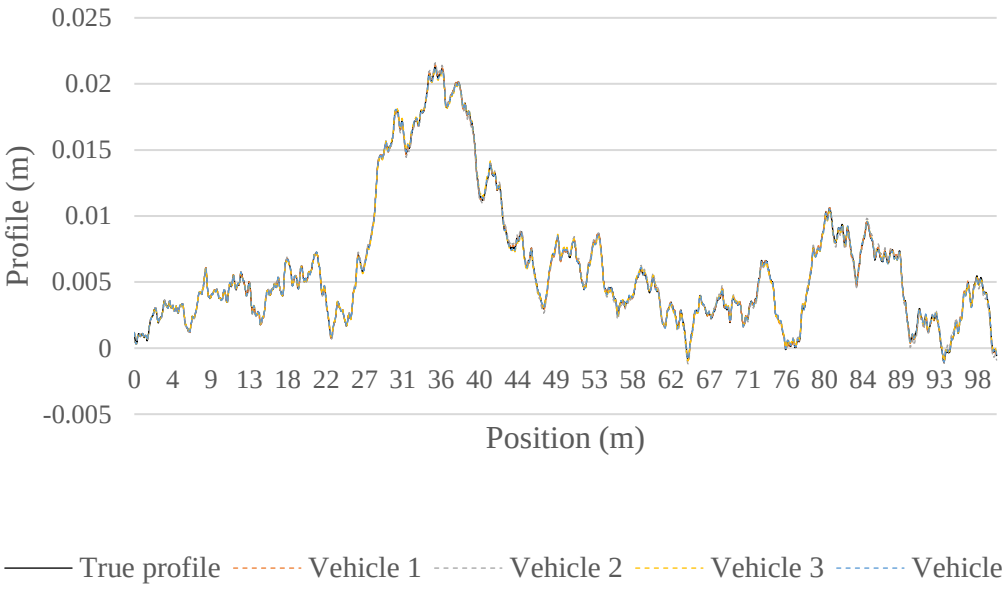

(a)

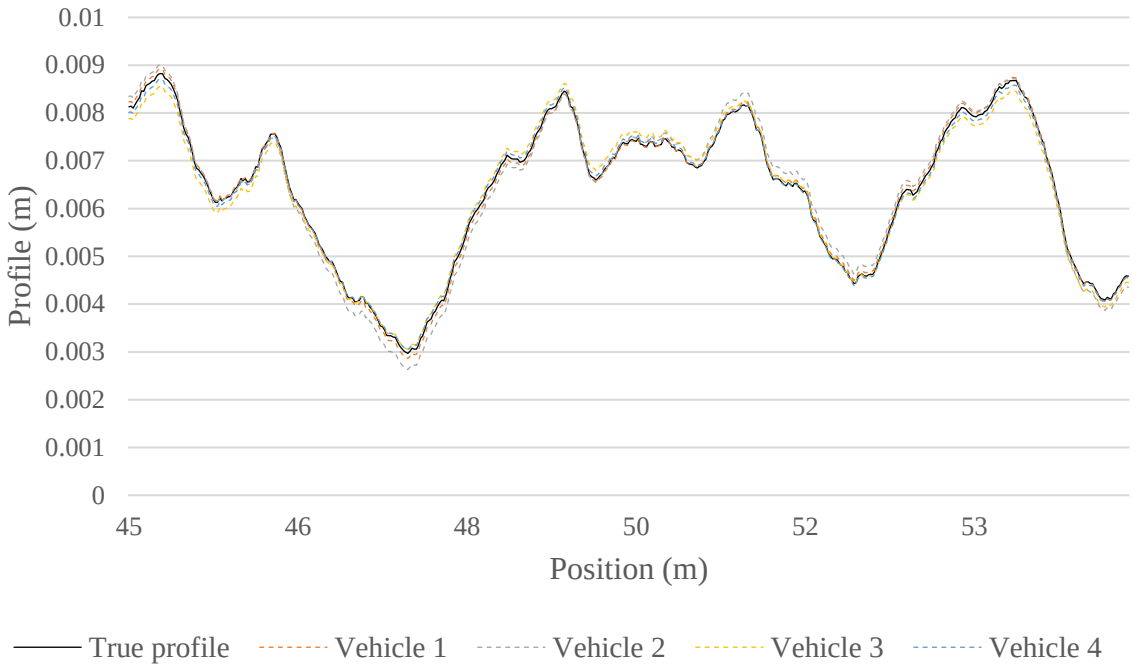

(b)

Figure 8(a). Calculated profile and true profile at Point A (0 to 100 m).

(b). Calculated profile and true profile at Point A (45 to 55 m).

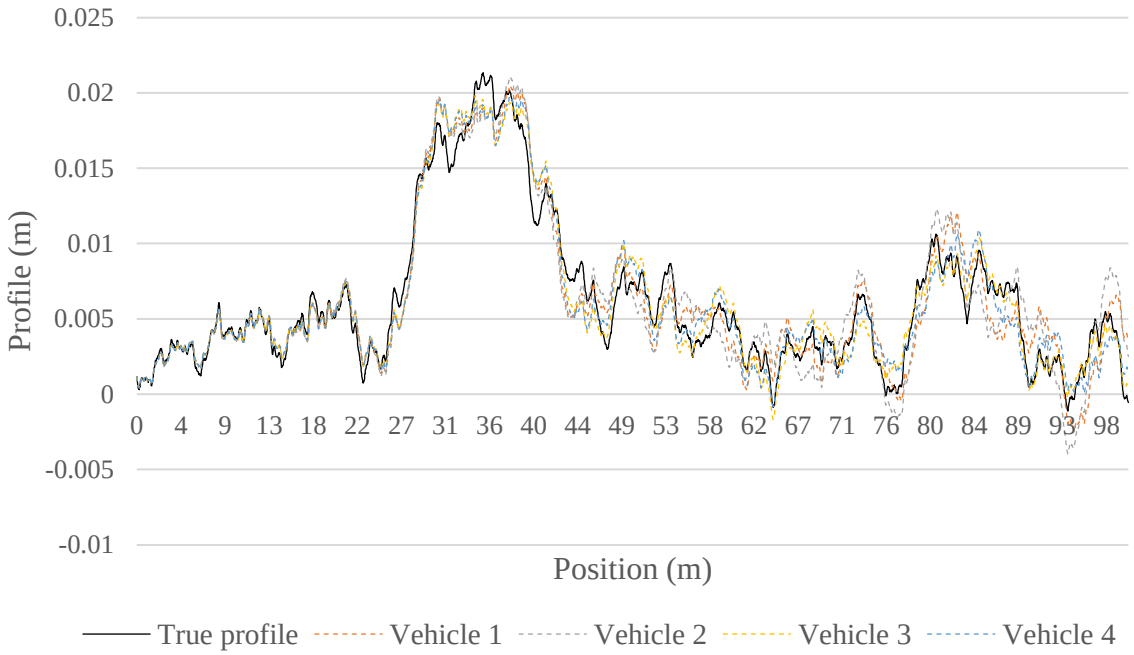

(a)

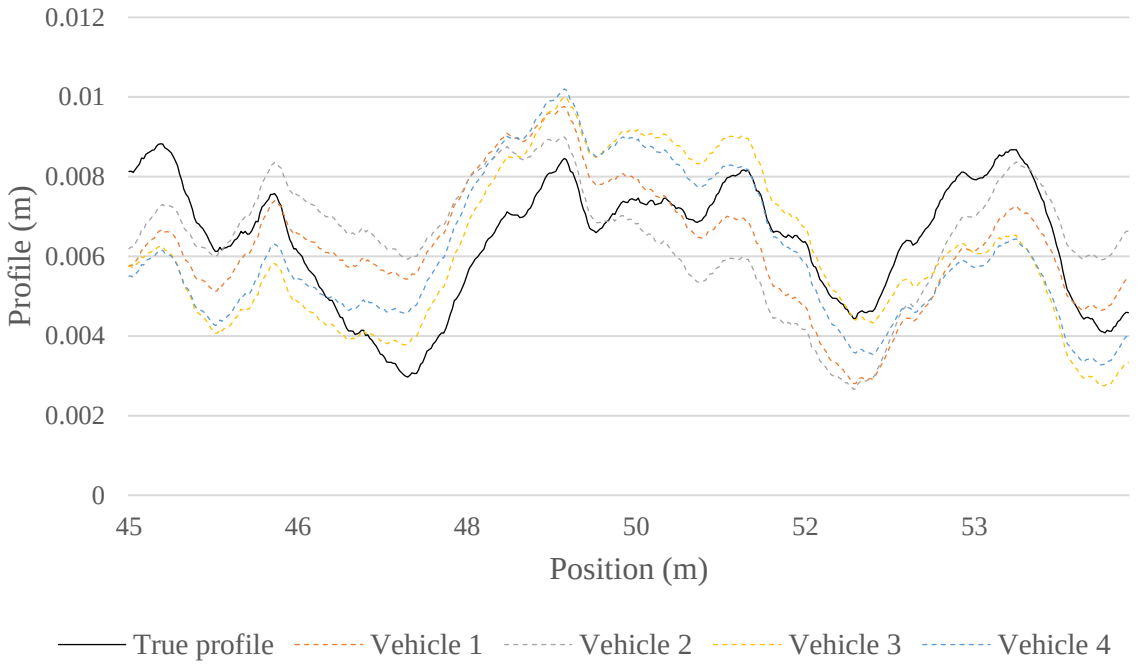

(b)

Figure 9(a). Calculated profile and true profile at Point B (0 to 100 m).

(b). Calculated profile and true profile at Point B (45 to 55 m).

Results for half-car model

The half-car model is further used to investigate the vehicle fleet concept. Vehicle properties for a fleet of six vehicles are randomly generated and are shown in Table 4. The forward problems are calculated to get sprung mass bounce acceleration and sprung mass pitch rotational velocity. From this the vehicle fleet problem is solved using these acceleration and velocity histories. The initial values for the properties of all vehicles are also shown in the table. The calculated profiles are shown in Figure 10. Figure 10(a) is the calculated profile for Vehicle 1 and the true profile. A detail in the 45 m to 55 m zone is shown in Figure 10(b). The calculated profiles for all six vehicles in the fleet and the true profile as shown in Figure 10(c).

Table 4. Vehicle properties and initial values.

	Vehicle 1	Vehicle 2	Vehicle 3	Vehicle 4	Vehicle 5	Vehicle 6	Initial values
I_s (kg m^2)	99 535	105 768	99 601	91 093	107 784	103 181	80 000
m_s (kg)	17 254	18 334	17 265	15 790	18 683	17 885	8000
$m_{u,1}$ (kg)	790	723	719	698	701	765	300
$m_{u,2}$ (kg)	1 223	1 228	1 156	1 120	956	1 110	800
$K_{s,1}$ (Nm^{-1})	381 764	390 569	408 043	378 317	380 460	383 341	300 000
$K_{s,2}$ (Nm^{-1})	1 053 990	974 042	993 026	1 055 407	1 097 135	1 121 343	800 000
$K_{t,1}$ (Nm^{-1})	1 763 507	1 648 493	1 957 895	1 848 174	1 924 673	1 537 987	1 000 000
$K_{t,2}$ (Nm^{-1})	3 694 467	3 340 706	3 666 718	3 392 386	3 271 068	3 960 334	2 000 000
$C_{s,1}$ (N sm^{-1})	11 720	9 178	10 633	10 037	9 605	9 119	9 000
$C_{s,2}$ (N sm^{-1})	16 367	21 888	21 262	20 034	23 745	17 528	10 000
D_1 (m)	2.375	2.375	2.375	2.375	2.375	2.375	2
D_2 (m)	2.375	2.375	2.375	2.375	2.375	2.375	2

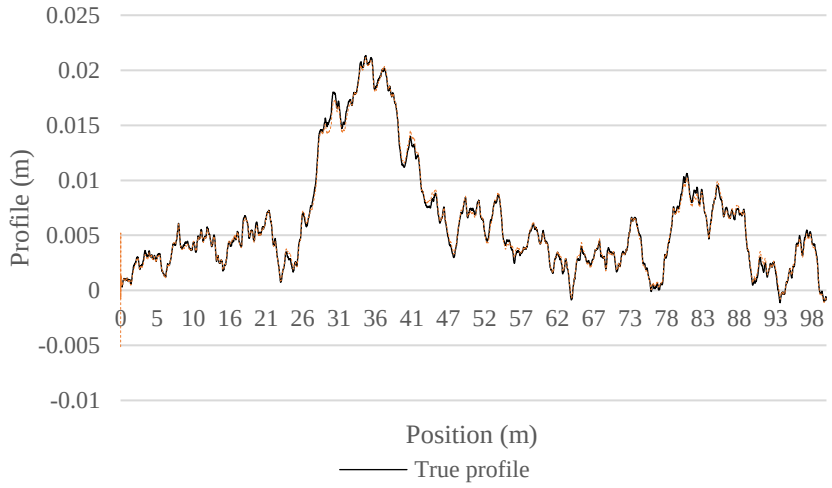

(a)

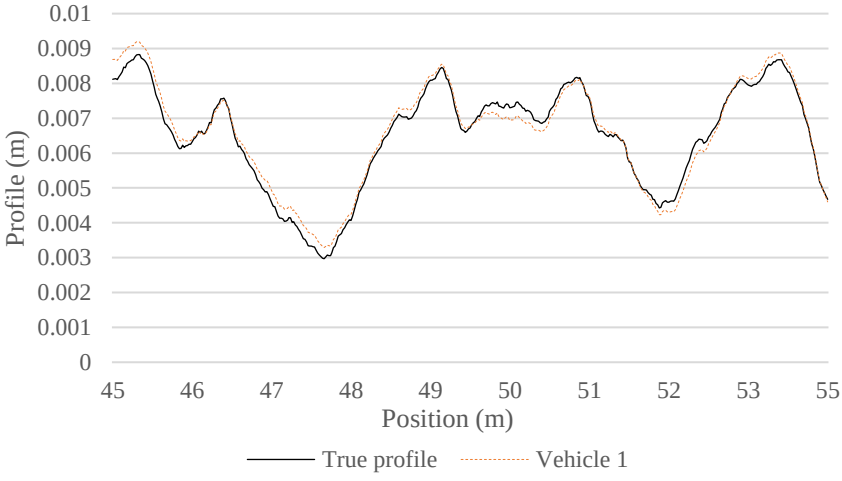

(b)

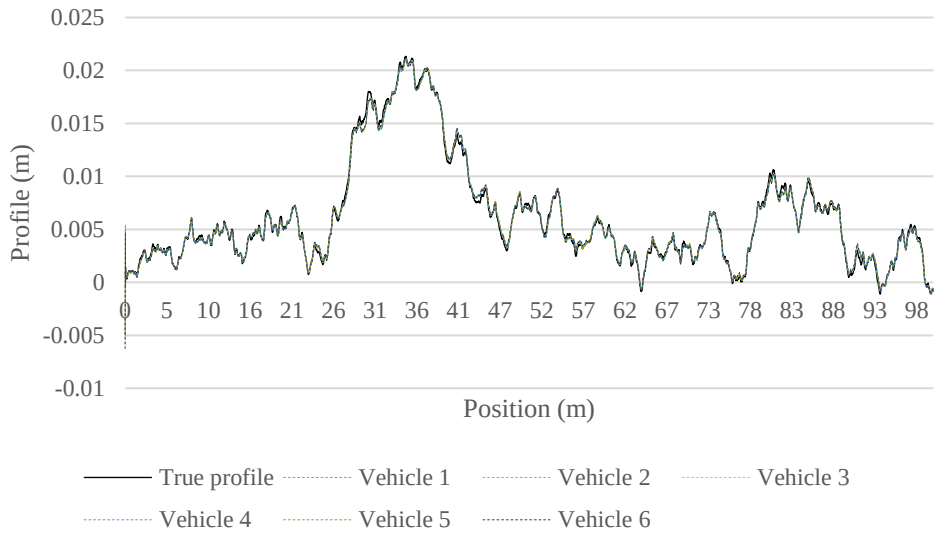

(c)

Figure 10(a). Calculated profiles of vehicle 1 and true profile (0 to 100 m). (b). Calculated profiles of vehicle 1 and true profile (45 to 55 m). (c). Calculated profiles of vehicle 1 to 6 and true profile (0 to 100 m).

Table 5 shows the calculated properties and error for each vehicle and the optimal set of properties. The errors for each vehicle are also illustrated in Figure 11. Like the sprung mass model results, the calculated vehicle properties are highly inaccurate though the calculated profiles are close to the 'true' profile. This method gives the best fit group of properties for every vehicle which successfully calculates the profiles. In Figure 11 the errors vary from -22% to +80%. Some results are consistent in their inaccuracy – for example D_1 is out by the same 9% for all vehicles. Others are highly variable – for example, $m_{u,2}$ varies from 24% to 80%.

Table 5. Calculated properties and error for each vehicle and properties.

	Vehicle 1	Error	Vehicle 2	Error	Vehicle 3	Error
I_s (kg m^2)	60 943	39%	69 047	35%	63 113	37%
m_s (kg)	10 259	41%	10 830	41%	10 043	42%
$m_{u,1}$ (kg)	418	47%	394	45%	373	48%
$m_{u,2}$ (kg)	929	24%	735	40%	699	39%
$K_{s,1}$ (kNm^{-1})	273 152	28%	289 817	26%	289 971	29%
$K_{s,2}$ (kNm^{-1})	704 855	33%	614 989	37%	682 622	31%
$K_{t,1}$ (kNm^{-1})	869 180	51%	827 021	50%	993 243	49%
$K_{t,2}$ (kNm^{-1})	1 799 818	51%	2 520 133	25%	2 454 087	33%
$C_{s,1}$ (N sm^{-1})	9 050	23%	7 460	19%	7 968	25%
$C_{s,2}$ (N sm^{-1})	11 621	29%	8 773	60%	9 686	54%
D_1 (m)	2.16	9%	2.16	9%	2.16	9%
D_2 (m)	2.54	-7%	2.73	-15%	2.69	-13%

	Vehicle 4	Error	Vehicle 5	Error	Vehicle 6	Error
I_s (kg m^2)	62 577	31%	68 551	36%	64 603	37%
m_s (kg)	10 406	34%	10 074	46%	10 204	43%
$m_{u,1}$ (kg)	399	43%	345	51%	414	46%
$m_{u,2}$ (kg)	779	30%	217	77%	217	80%
$K_{s,1}$ (kNm^{-1})	299 588	21%	259 326	32%	274 102	28%
$K_{s,2}$ (kNm^{-1})	795 842	25%	681212	38%	662 886	41%
$K_{t,1}$ (kNm^{-1})	1 026 031	44%	924710	52%	745 038	52%
$K_{t,2}$ (kNm^{-1})	1 598 121	53%	1893572	42%	1 748 962	56%
$C_{s,1}$ (N sm^{-1})	8 382	16%	6 958	28%	7 206	21%
$C_{s,2}$ (N sm^{-1})	11 317	44%	12 213	49%	14 346	18%
D_1 (m)	2.16	9%	2.16	9%	2.17	9%
D_2 (m)	2.56	-8%	2.90	-22%	2.69	-13%

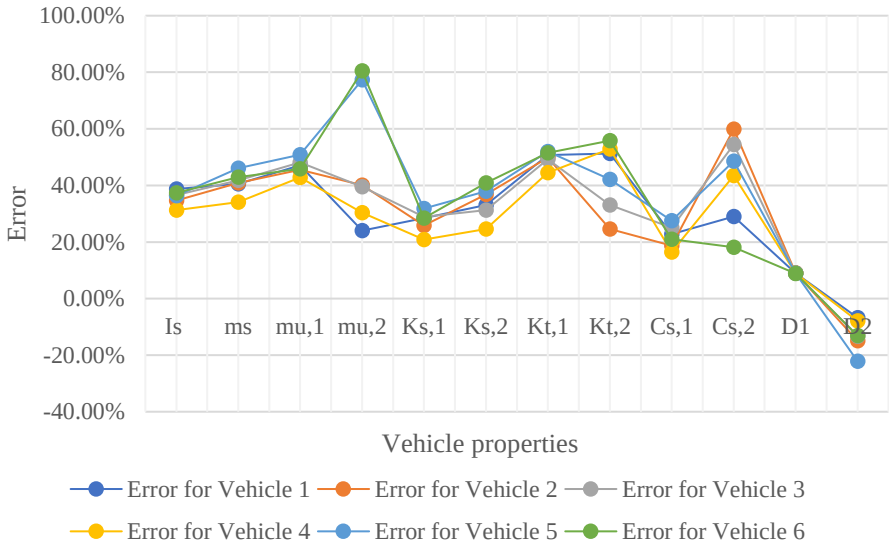

Figure 11. Errors in vehicle properties.

Implications of noise in accelerations

In this section, Additive White Gaussian Noise (AWGN) is added to allow for inaccuracy in the acceleration measurements. Noise is added to the accelerations according to Equation (34) (Lyons, 2011):

$$A_{polluted} = A + E_{noise} \times Noise \tag{34}$$

where $A_{polluted}$ is the acceleration with noise, A is the original acceleration without noise, $Noise$ is a standard normal distribution vector with zero mean and unit standard deviation and E_{noise}^2 is the square of the energy in the noise. The E_{noise}^2 is calculated from the definition of the *SNR* given by Equation (35):

$$SNR = 10\, log_{10} \frac{var(A)}{E_{noise}^2} \tag{35}$$

which is the ratio of the power in the signal to the power in the noise, where $var(A)$ is the variance of the acceleration signal. Here, the 'measured' accelerations are contaminated

assuming 1% noise (signal-to-noise ratio, *SNR*=100). Figure 12 (a) shows the calculated profile for Vehicle 1 while Figure 12 (b) shows the calculated profiles for all six vehicles in the fleet. A detail in the 45 m and 55 m zone is shown in Figure 12 (c). The true profile is also shown in all figures. While the noise clearly has an influence, the calculated profile is reasonably close to the true one. Figure 12 (b) shows that the profiles inferred from the population of six vehicles are similar. This is a feature of the strategy described in Equation (32), namely, that similar profiles are assumed to be more likely to be correct. Furthermore, different levels of noise are added to accelerations to study its effects. The calculated profiles are determined and analysed by Root Mean Square Error (RMSE). The RMSE for each calculated profile under different noise are calculated using the equation:

$$RMSE = \sqrt{\frac{1}{N}\sum_{k=1}^{N}(r_{true,k} - \bar{r}_{calculated,k})^2}$$

where $r_{true,k}$ is the true profile at the k^{th} point, $\bar{r}_{calculated,k}$ is the mean of 6 calculated profiles at the k^{th} point. RMS errors for different noise levels are calculated using this equation and the results are shown in Figure 13. It can be seen that the RMS errors increase with increasing noise level, but a reasonable level of accuracy is maintained. It is felt by the authors that the influence of noise will be much reduced when larger populations are considered.

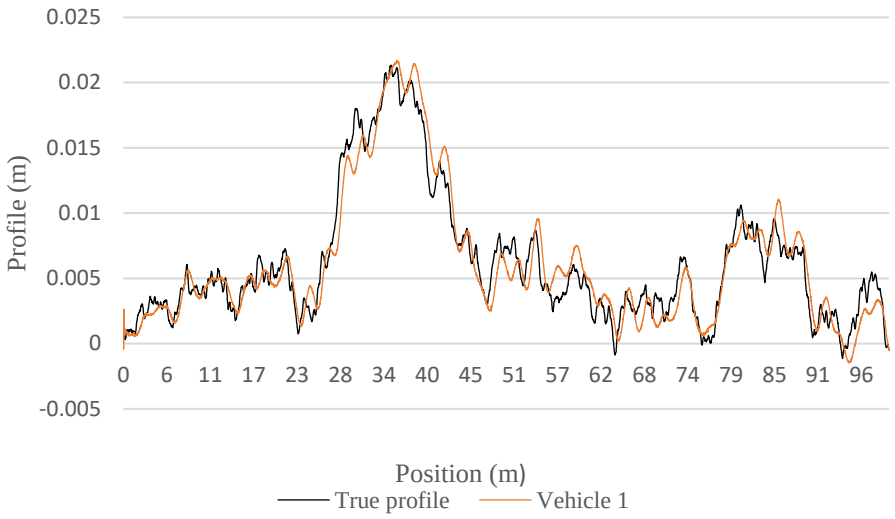
0.025
0.02
0.015
0.01
0.005
0
-0.005
Profile (m)
0 6 11 17 23 28 34 40 45 51 57 62 68 74 79 85 91 96
Position (m)
True profile
Vehicle 1

(a)

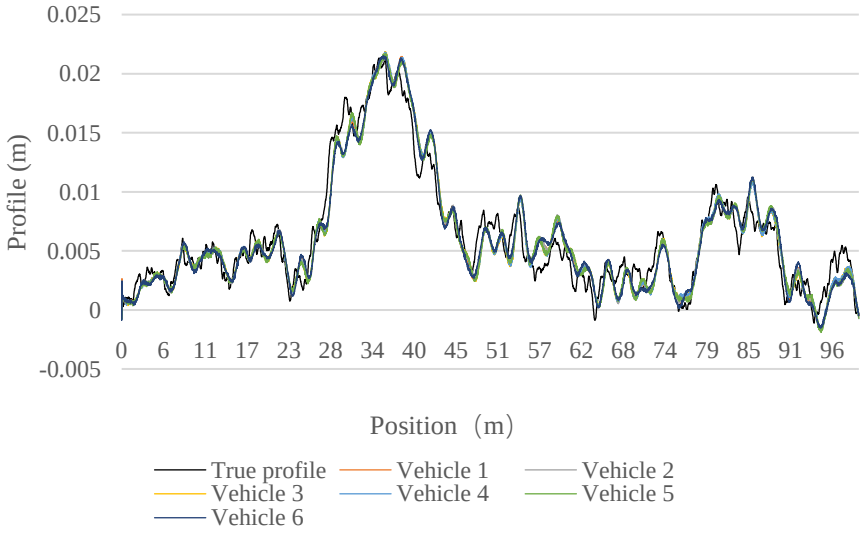
0.025
0.02
0.015
0.01
0.005
0
-0.005
Profile (m)
0 6 11 17 23 28 34 40 45 51 57 62 68 74 79 85 91 96
Position（m）
True profile
Vehicle 1
Vehicle 2
Vehicle 3
Vehicle 4
Vehicle 5
Vehicle 6

(b)

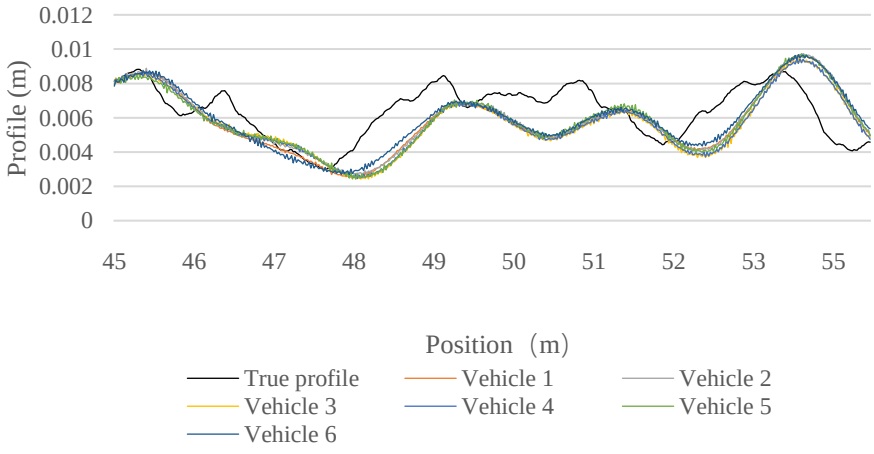
0.012
0.01
0.008
0.006
0.004
0.002
0
Profile (m)
45 46 47 48 49 50 51 52 53 55
Position（m）
True profile
Vehicle 1
Vehicle 2
Vehicle 3
Vehicle 4
Vehicle 5
Vehicle 6

(c)

Figure 12 (a). Calculated profiles of vehicle 1 and true profile in the presence of noise. (b). Calculated profiles of vehicle 1 to 6 and true profile in the presence of noise (0 to 100 m). (c). Calculated profiles of vehicle 1 to 6 and true profile in the presence of noise (45 to 55m).

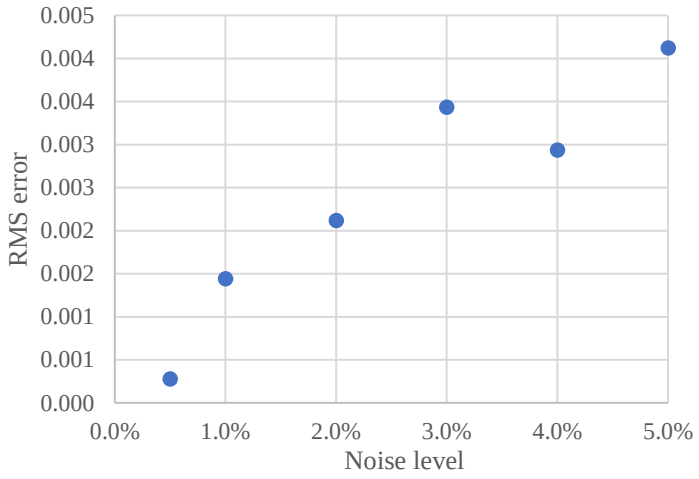

Figure 13. RMS errors of calculated profile for different noise levels.

Conclusions and future work

This paper introduces a novel method of inferring road or rail surface profiles from inertial measurements. A new direct integration approach is proposed to determine the profiles using accelerations measured in passing vehicles. The acceleration histories are simulated here using a vehicle/road dynamic interaction model. Sprung mass and half-car models are tested separately. The results show that the calculated profiles are the same as the true profiles used in the forward problem to generate the accelerations. The direct integration approach is much more efficient than optimization and allows the calculation to be completed rapidly.

The work is expanded to introduce the concept of using a fleet of vehicles to determine a profile. Using several vehicles, the profiles can be calculated without prior knowledge of the vehicle properties in a process that combines the direct integration approach with CE optimisation. The results show that the algorithm is successful in predicting profiles that are

similar to the true profile. The vehicle properties are inaccurate when estimated from the road profile, but some characteristics such as mass and stiffness ratios in the sprung-mass model are accurately captured, which results in good accuracy for road profile estimation.

To process data from a vehicle fleet will require the solution of an inverse dynamics problem, the calibration of a fleet of vehicles and the use of the database of accelerations to determine bridge conditions in the future.

Acknowledgments

Mr. Yifei Ren acknowledges the Ph.D. scholarship awarded jointly by University College Dublin and the China Scholarship Council.

References:

Ben Hassen, D., Miladi, M., Abbes, M. S., Baslamisli, S. C., Chaari, F., & Haddar, M. (2019). Road profile estimation using the dynamic responses of the full vehicle model. *Applied Acoustics, 147*, pp. 87-99.

Botev, Z., & Kroese, D. P. (2004) *Global likelihood optimization via the CE method, with an application to mixture models*. Paper presented at the Proceedings of the 36th conference on Winter simulation, Washington, DC, USA.

Casero, M., González, A., & Covián, E. (2014) *Finite Element Updating using Cross-Entropy combined with Random Field Theory*. Paper presented at the The Twelfth International Conference on Computational Structures Technology (CST 2014), Naples, Italy.

Elhattab, A., Uddin, N., & OBrien, E. J. (2016). Drive-by bridge damage monitoring using Bridge Displacement Profile Difference. *Journal of Civil Structural Health Monitoring, 6*(5), pp. 839-850.

Ergun, M., Iyinam, S., & Iyinam, A. F. (2005). Prediction of Road Surface Friction Coefficient Using Only Macro- and Microtexture Measurements. *JOURNAL OF TRANSPORTATION ENGINEERING, 131*(4), pp. 311-319.

Fauriat, W., Mattrand, C., Gayton, N., Beakou, A., & Cembrzynski, T. (2016). Estimation of road profile variability from measured vehicle responses. *Vehicle System Dynamics, 54*(5), pp. 585-605.

Flintsch, G. W., Ferne, B., Diefenderfer, B., Katicha, S., Bryce, J., & Nell, S. (2012) *Valuation of traffic speed continuous deflection devices*. Paper presented at the 91st Annual Meeting, Transport Research Board, USA.

Fox, A., Kumar, B. V. K. V., Chen, J., & Bai, F. (2017). Multi-Lane Pothole Detection from Crowdsourced Undersampled Vehicle Sensor Data. *IEEE Transactions on Mobile Computing, 16*(12), pp. 3417-3430.

Goldberg, D. E., & Holland, J. H. (1988). Genetic algorithms and machine learning. *Machine Learning, 3*, pp. 95-99.

González, A., OBrien, E. J., Li, Y. Y., & Cashell, K. (2008). The use of vehicle acceleration measurements to estimate road roughness. *Vehicle System Dynamics, 46*(6), pp. 483-499.

Harris, N. K., Gonzalez, A., OBrien, E. J., & McGetrick, P. (2010). Characterisation of pavement profile heights using accelerometer readings and a combinatorial optimisation technique. *Journal of Sound and Vibration, 329*(5), pp. 497-508.

Harris, N. K., OBrien, E. J., & González, A. (2007). Reduction of bridge dynamic amplification through adjustment of vehicle suspension damping. *Journal of Sound and Vibration, 302*(3), pp. 471-485.

Imine, H., Delanne, Y., & M'Sirdi, N. K. (2006). Road profile input estimation in vehicle dynamics simulation. *Vehicle System Dynamics, 44*(4), pp. 285-303.

ISO-8608. (1995). Mechanical vibration-road surface profiles-reporting of measured data. International Organization for Standardization (ISO), Geneva.

Kim, C. W., Isemoto, R., Toshinami, T., Kawatani, M., McGetrick, P., & OBrien, E. J. (2011) *Experimental investigation of drive-by bridge inspection*. Paper presented at the 5th International Conference on Structural Health Monitoring of Intelligent Infrastructure (SHMII-5), Cancun, Mexico.

Li, W., Jiang, Z., Wang, T., & Zhu, H. (2014). Optimization method based on Generalized Pattern Search Algorithm to identify bridge parameters indirectly by a passing vehicle. *Journal of Sound and Vibration, 333*(2), pp. 364-380.

Lin, C. W., & Yang, Y. B. (2005). Use of a passing vehicle to scan the fundamental bridge frequencies: An experimental verification. *Engineering Structures, 27*(13), pp. 1865-1878.

Lyons, R. G. (2011). Understanding Digital Signal Processing (3rd ed.) Boston, MA, USA: Prentice Hall.

Ma, L., Li, Y., Li, J., Wang, C., Wang, R., & Chapman, M. (2018). Mobile Laser Scanned Point-Clouds for Road Object Detection and Extraction: A Review. *Remote Sensing, 10*(10), p 1531.

Malekjafarian, A., Martinez, D., & OBrien, E. J. (2017) *Pavement condition measurement at high velocity using a TSD*. Paper presented at the 27th annual European Safety and Reliability Conference (ESREL 2017), Portoroz, Slovenia.

Malekjafarian, A., McGetrick, P. J., & OBrien, E. J. (2015). A Review of Indirect Bridge Monitoring Using Passing Vehicles. *Shock and Vibration, 2015*, pp. 1-16.

McGetrick, P. J., González, A., & Obrien, E. J. (2009). Theoretical investigation of the use of a moving vehicle to identify bridge dynamic parameters. *Insight - Non-Destructive Testing and Condition Monitoring, 51*(8), pp. 433-438.

O'Leary, D. E. (2013). Exploiting Big Data from Mobile Device Sensor-Based Apps: Challenges and Benefits. *MIS Quarterly Executive, 12*(4), pp. 179-187.

OBrien, E. J., & Keenahan, J. (2015). Drive-by damage detection in bridges using the apparent profile. *Structural Control and Health Monitoring, 22*(5), pp. 813-825.

OBrien, E. J., McGetrick, P. J., & Gonzalez, A. (2014). A drive-by inspection system via vehicle moving force identification. *Smart Structures and Systems, 13*(5), pp. 821-848.

Quirke, P., Cantero, D., OBrien, E. J., & Bowe, C. (2016). Drive-by detection of railway track stiffness variation using in-service vehicles. *Proceedings of the Institution of Mechanical Engineers, Part F: Journal of Rail and Rapid Transit, 231*(4), pp. 498-514.

Rubinstein, R. Y., & Kroese, D. P. (2004). *The Cross-Entropy Method: A Unified Approach to Combinatorial Optimization, Monte-Carlo Simulation and Machine Learning* New York: Springer-Verlag.

Sattar, S., Li, S., & Chapman, M. (2018). Road Surface Monitoring Using Smartphone Sensors: A Review. *Sensors (Basel), 18*(11)Retrieved from https://www.ncbi.nlm.nih.gov/pubmed/30423962

Sayers, M. W., & Karamihas, S. M. (1996). *Interpretation of road profile roughness data*: University of Michigan Transportation Research Institute, UMTRI-96-19.

Sayers, M. W., & Karamihas, S. M. (1998). *The little book of profiling*: University of Michigan Transportation Research Institute, UMTRI-96-19.

Souza, V. M. A., Giusti, R., & Batista, A. J. L. (2018). Asfault: A low-cost system to evaluate pavement conditions in real-time using smartphones and machine learning. *Pervasive and Mobile Computing, 51*, pp. 121-137.

Walsh, B. J., & González, A. (2009). Assessment of the Condition of a Beam Using a Static Loading Test. *Key Engineering Materials, 413-414*, pp. 269-276.

Wang, Z., Dong, M., Qin, Y., Du, Y., Zhao, F., & Gu, L. (2016). Suspension system state estimation using adaptive Kalman filtering based on road classification. *Vehicle System Dynamics, 55*(3), pp. 371-398.

Yang, Y. B., Li, Y. C., & Chang, K. C. (2014). Constructing the mode shapes of a bridge from a passing vehicle: a theoretical study. *Smart Structures and Systems, 13*(5), pp. 797-819.

Yang, Y. B., & Lin, C. W. (2005). Vehicle–bridge interaction dynamics and potential applications. *Journal of Sound and Vibration, 284*(1-2), pp. 205-226.

Yang, Y. B., Lin, C. W., & Yau, J. D. (2004). Extracting bridge frequencies from the dynamic response of a passing vehicle. *Journal of Sound and Vibration, 272*(3-5), pp. 471-493.

Zang, K., Shen, J., Huang, H., Wan, M., & Shi, J. (2018). Assessing and Mapping of Road Surface Roughness based on GPS and Accelerometer Sensors on Bicycle-Mounted Smartphones. *Sensors (Basel), 18*(3)